nBn detectors based on InAs/GaSb type-II strain layer superlattice

G. Bishop, E. Plis,[a] J. B. Rodriguez, Y. D. Sharma, H. S. Kim,
L. R. Dawson, and S. Krishna
Center for High Technology Materials, University of New Mexico, 1313 Goddard Street SE, Albuquerque, New Mexico 87106

(Received 26 October 2007; accepted 3 December 2007; published 30 May 2008)

We report on a type-II InAs/GaSb strain layer superlattice photodetector using a nBn design with cutoff wavelength of ~4.8 μm at 250 K. The surface component of dark current was eliminated. Using a shallow isolation etch, low temperature dark current was reduced by two orders of magnitude compared with conventional photodiode processing. Dark current densities were equal to 2.3×10^{-6} and 3.1×10^{-4} A/cm^2 (V_b=0.1 V, T=77 K) for detectors with shallow isolation etch and conventional defined mesa, respectively. Quantum efficiency, responsivity, and spectral detectivity D^* of the device are presented. © *2008 American Vacuum Society.* [DOI: 10.1116/1.2830627]

The detection of midwavelength infrared radiation (MWIR) is very important for many military, industrial, and biomedical applications. Present-day commercially available uncooled IR sensors operating in MWIR region (3–5 μm) use microbolometer detectors, which are inherently slow and less sensitive. Available photon detectors [mercury cadmium telluride (MCT) and quantum well infrared detectors (QWIPs)] overcome this limitation. However, MCT detectors are characterized by low electron effective mass resulting in excessive dark current due to tunneling.[1] In accordance with the absorption selection rules, QWIPs cannot couple photon at normal incidence. Moreover, quantum efficiency of QWIPs is low due to the small volume of active region. Due to these reasons, present-day MWIR detectors need to be cooled to cryogenic temperatures (77–100 K) in order to operate at background limited infrared photodetection (BLIP) conditions. The requirement of cooling limits the lifetime, increases the weight and the total cost, as well as the power budget of the whole infrared system.

Proposed by Smith and Mailhiot[2] in 1980s, detectors based on InAs/GaSb superlattices (SLs) have attracted a lot of attention over the past few years as a possible alternative to the present-day IR detection systems. The effective mass of the superlattice is not dependent on the band gap as in the case in bulk semiconductor material. The larger effective mass in SLs leads to a reduction of tunneling currents. Large splitting between heavy-hole and light-hole valence subbands due to strain in the SLs contributes to the suppression of Auger recombination. This makes detectors based on SLs attractive for realization of high performance infrared sensors operating at high temperature.

Presently, all SL detectors are based on a photodiode design. At cryogenic temperature, the major sources of noise for photodiode are recombination at Shockley-Read-Hall centers and surface states. In order to eliminate surface leakage currents, different passivation methods have been investigated, such as deposition of relatively thick layer of dielectric material,[3] polyamide passivation,[4] overgrowth of wide band gap material,[5] deposition of passivating sulfur coating electrochemically,[6] and from chemical solutions.[7] All of these methods add complexity to the fabrication. In addition, long-term reliability of these methods has not been studied yet.

Recently, a new heterostructure design with extremely low surface currents has been proposed.[8] This so-called nBn structure consists of a *n*-type narrow band-gap contact and absorber layers separated by a 50–100 nm thick wide band gap barrier layer. A 100 K increase in the BLIP temperature was demonstrated. Rodriguez *et al.*[9] reported the implementation of nBn design for InAs/GaSb MWIR SL detectors. Devices showed values of quantum efficiency and shot-noise-limited specific detectivity comparable to the state-of-the-art *p-i-n* diodes based on the SLs. However, no detailed study on surface current reduction mechanism as well as optimization of detector structure was performed that time. In this article, we present nBn detector structure based on type-II SL material that demonstrates promising results for suppression of surface leakage currents due to device design and processing. We found dark current at 77 K was reduced by two orders of magnitude due to elimination of surface currents in comparison with conventional photodiode processing.

The structures presented in this article were grown on Te-doped GaSb (001) substrates by solid source molecular beam epitaxy in a VG-80 system equipped with an arsenic valved cracker source, an antimony cracker source, and Ga and In SUMO® cells. A detailed description of growth procedure has been reported elsewhere.[10,11] Device consists of 0.25 μm thick *n*-type bottom contact layer composed of 8 ML InAs:Si ($n=4\times10^{18}$ cm^{-3})/8 ML GaSb SLs followed by the nonintentionally doped 1.4 μm thick 8 ML InAs/8 ML GaSb absorber layer. An $Al_{0.2}Ga_{0.8}Sb$ barrier layer with thickness of 100 nm was then grown on the top of absorber layer. In an nBn structure, the function of heterojunction barrier is to block the flow of majority carriers through the device. Composition of the barrier was chosen in such a way that the majority carrier current (electron current) is blocked whereas the minority carrier current (hole current) can flow

[a]Electronic mail: alien@chtm.unm.edu

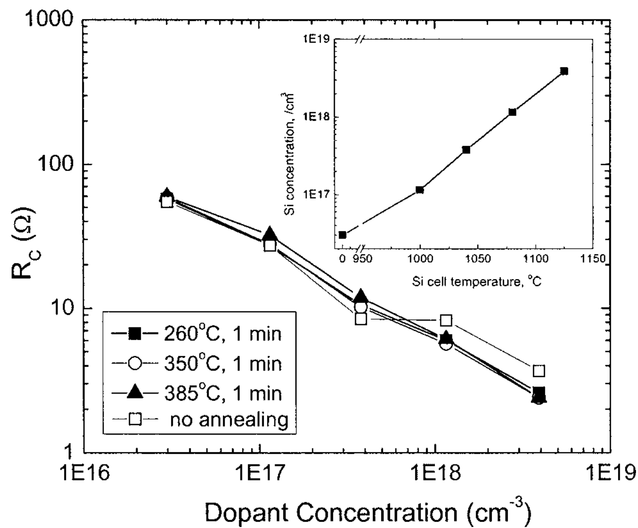

FIG. 1. Resistance vs the doping concentration in the contact layer at different annealing temperatures for Ti/Pt/Au contacts on *n*-type InAs/GaSb superlattice. Inset: the doping concentration as a function of the Si cell temperature.

unimpeded because the valence band offset with surrounding SL layers is minimized. However, due to the uncertainty involved with the SL modeling, the exact band offsets are difficult to determine. The barrier layer was grown to be thick enough to prevent electron tunneling from the top contact SL layer to the SL absorbing layer. The structure was capped by 100 nm thick top contact layer with the same superlattice composition, thickness, and doping concentration as the bottom contact layer. Heavily doped contact layers were used in order to ensure Ohmic behavior of the contacts. The structural properties were assessed by high-resolution x-ray diffraction which shows that the SL material appears lattice matched to the substrate within 0.05%, while the AlGaSb layer peak is located at around 0.27% in compressive strain.

The nBn structure is designed to operate with *n*-type layers in flatband or with a little depletion. Since the Shockley-Read-Hall (SRH) generation-recombination current is associated with depletion region of photodiodes, nBn design essentially eliminates the SRH currents. However, in our structure absorber and bottom contact layers consist of the same SLs and the doped SLs, contact layer forms the *n*-*n*+ homojunction with nominally undoped absorber layer. In this case, space-charge region is created and the SRH current could contribute to the dark current. In order to reduce the SRH current, doping concentration in the contact layer needs to be decreased while maintaining good Ohmic contact.

To optimize the doping level of the bottom contact layer, several $\sim 0.5\ \mu$m thick structures consisting of 8 ML InAs:Si/8 ML GaSb SLs with different doping levels were grown. Doping concentrations as a function of dopant cell (Si) temperature are presented in the inset to Fig. 1. Transmission line method (TLM) patterns were defined by conventional UV lithography. The interspacing between the metal pads varied from 10 to 70 μm and the dimensions of the metal pads were $50 \times 100\ \mu\text{m}^2$. Commonly used Ti 500 Å/Pt 500 Å/Au 3000 Å metallization was utilized for the contacts. Samples were annealed using the following conditions: (I) no annealing, (II) 260 °C, 1 min, (III) 350 °C 1 min, and (IV) 385 °C 1 min. The results are summarized in Fig. 1.

Ti/Pt/Au metallization on undoped SL material ($n=3 \times 10^{16}$ cm^{-3}) did not lead to the Ohmic behavior in the current-voltage characteristics. Contact resistance was found to be $\sim 55\ \Omega$ regardless of annealing temperature. With increased level of doping concentration in the SL layer, the Ohmic behavior in the current-voltage characteristics was observed and contact resistance was improved. Structure with the highest investigated doping level ($n=4 \times 10^{18}$ cm^{-3}) demonstrated contact resistance equal to 3.7 Ω (no annealing) and 2.4 Ω (annealing at 350 °C during 1 min). Annealing at 380 °C did not considerably improve the contact resistance of investigated contacts whereas surface metal layer was degraded. The results indicate that doping concentration needs to exceed 1×10^{18} cm^{-3} in order to realize Ohmic contact to *n*-type InAs/GaSb SLs. Thus, in order to obtain Ohmic contacts to the InAs/GaSb SL at lower doping concentrations of contact layer, we need to use a different metallization. GeAu-based metallization on the *n*-type GaSb have been shown to provide good Ohmic contacts by combination of the advantages of solid phase reactions of Ge-based contacts with a low Ohmic resistance of the Au-based contacts.[11] For the contact resistance study, an $\sim 0.5\ \mu$m thick SL sample with the 8 ML InAs:Si/8 ML GaSb ($n=5 \times 10^{17}$ cm^{-3}) was grown. After Ge/Au/Pt/Au (287/568/504/2000 Å) contact was deposited, sample was annealed at 380 °C during 1 min. TLM measurements revealed contact resistance equal to 1 Ω which indicates a good Ohmic contact.

We are currently undertaking experiments by varying the materials, thickness of each component of the metallization, and the annealing temperature in order to further optimize contact resistance. We will incorporate the results of our study in the next batch of nBn SL structures. In the presented devices, we used highly doped bottom contact ($n=4 \times 10^{18}$ cm^{-3}) and Ti/Pt/Au (500/500/3000 Å) metallization. Since we found postannealing improvement in contact resistance only by factor of 1.5, the heat treatment of contacts was omitted.

The devices were processed into two distinct structures (further referred as structures A and B) using $400 \times 400\ \mu\text{m}^2$ square mesas with circle apertures ranging from 25 to 300 μm. Processing was initiated by standard optical photolithography for top contact metal deposition. We used Ti/Pt/Au (500/500/3000 Å) as contact metals for both top and bottom contact metallizations. Then, an isolation etch was undertaken using H_3PO_4:H_2O_2:H_2O solution (1:2:20) to the middle of the barrier layer for structure A (etch depth ~ 0.15 nm). Then, inductively coupled plasma dry etch to the middle of the bottom contact layer was performed for both structures A and B. Finally, samples were patterned and bottom contact metal was deposited. Schematics of processed structures A and B are shown in the Fig. 2.

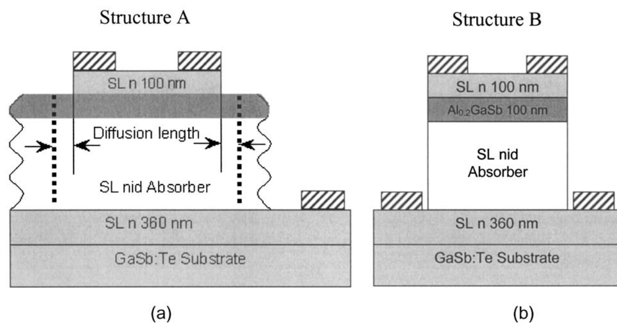

FIG. 2. (a) Schematic of shallow etched isolation device (structure A). The active area is defined by the diffusion length of the minority carriers (holes). (b) Conventionally defined mesa (structure B).

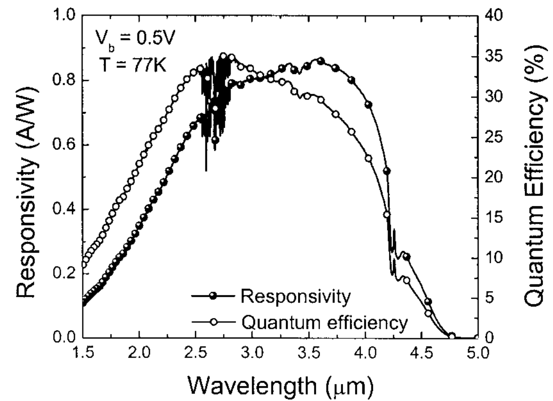

FIG. 4. The responsivity and quantum efficiency vs the wavelength for structure A measured at 77 K with V_b=0.5 V.

For structure A, the active area of the devices is defined by the diffusion length of minority carriers (holes) rather than by a conventional mesa. For structure B, dangling bonds are presented on the etched mesa sidewalls and surface leakage current is expected to be high.

After processing, devices were wire bonded to a leadless chip carrier for further characterization. Current-voltage characteristics were measured in the 77–293 K range with a room temperature background illumination using HP4145 semiconductor parameter analyzer. For the nBn detector structure, forward bias is defined as a positive voltage applied to the bottom contact of the detector. The dark current densities measured at V=0.1 V for structures A and B as a function of temperature are shown in the Fig. 3. Ratio of dark current densities measured at the same value of applied bias for both structures is also shown. At high temperature, the thermally generated carriers dominate the dark current and the influence of the surface current component is not seen as the size of the mesa is large. Since bulk component of dark current is strongly temperature dependent, as the temperature decreases, the surface current becomes the dominant component of dark current at low temperatures. Consequently, the levels of dark current in structures A and B are comparable at 250 K but the dark current in structure A is reduced by two orders of magnitude at 77 K. Dark current densities were equal to 2.3×10^{-6} and 3.1×10^{-4} A/cm^2 for structures A and B, respectively, at V_b=0.1 V and T=77 K. At 250 K, the dark current density was equal to ~80 mA/cm^2 for devices with isolation mesa etch.

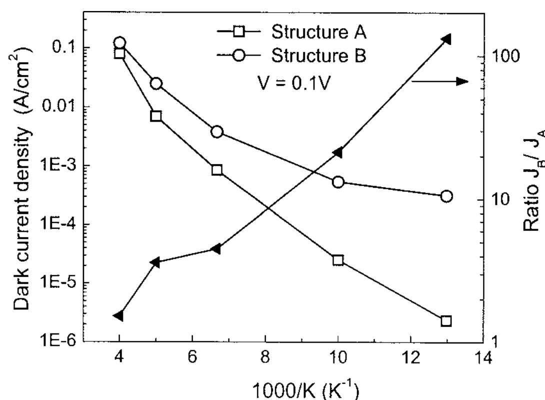

FIG. 3. The dark current density vs 1000/T in structures A and B (V_b =0.1 V). The ratio of dark current densities for both structures measured at the same value of applied bias is also shown.

Temperature dependent spectral response of structure A was measured using Nicolet 670 Fourier transform infrared spectrometer. The spectral response was clearly visible up to 250 K (V_b=0.5 V). The cutoff wavelength was shifted from ~4.2 μm at 77 K to ~4.8 μm at 250 K. A Micron M365 Calibrated Blackbody Source at 500 °C was used to measure the responsivity and quantum efficiency (QE) of the device (Fig. 4). The measurements show maximum values of current responsivity and QE of 0.74 A/W and 23% at 4.0 μm, respectively. No anti-reflection coating was applied on the device.

The shot-noise limited spectral detectivity D^* of the device was estimated using

$$D^* = R/\sqrt{2qJ + (4kT)/(R_d A_d)}, \quad (1)$$

where R is the responsivity, q is the electronic charge, T is the temperature of the device, k is Boltzmann's constant, J is the current density, R_d is the dynamic resistance, and A_d is the diode area. At 77 K, the maximum D^* was equal to 2.8×10^{11} Jones (V_b=0.5 V, λ=4 μm).

In conclusion, we report a nBn detector based on InAs/GaSb SLs with cutoff wavelength of ~4.8 μm at 250 K. Due to the way devices were defined and processed, low temperature dark current was reduced by two orders of magnitude due to elimination of surface currents in comparison with conventional photodiode processing. Dark current densities were equal to 2.3×10^{-6} and 3.1×10^{-6} A/cm^2 for detectors with shallow etch defined mesa (structure A) and conventionally defined mesa (structure B), respectively. At 250 K, the dark current density was equal to ~80 mA/cm^2 for devices with isolation mesa etch. Removal of surface currents is an important milestone for fabrication of high performance focal plane arrays based on InAs/GaSb SLs and operating in MWIR, LWIR, and VLWIR regions.

This work was supported by DARPA HOT MWIR.

[1]A. Rogalski, Rep. Prog. Phys. **68**, 2267 (2005).
[2]D. L. Smith and C. Mailhiot, J. Appl. Phys. **62**, 2545 (1987).
[3]A. Gin, Y. Wei, J. Bae, A. Hood, J. Nah, and M. Razeghi, Thin Solid Films **447–448**, 489 (2004).
[4]A. Hood, P.-Y. Delaunay, D. Hoffman, B.-M. Nguyen, Y. Wei, and M. Razeghi, Appl. Phys. Lett. **90**, 233513 (2007).
[5]R. Rehm, M. Walther, F. Fuchs, J. Schmitz, and J. Fleibner, Appl. Phys. Lett. **86**, 173501 (2005).
[6]E. Plis, J. B. Rodriguez, S. J. Lee, and S. Krishna, Electron. Lett. **42**, 1248 (2006).
[7]A. Gin, Y. Wei, A. Hood, A. Bajowala, V. Yazdanpanah, and M. Razeghi, Appl. Phys. Lett. **84**, 2037 (2004).
[8]S. Maimon and G. W. Wicks, Appl. Phys. Lett. **89**, 151109 (2006).
[9]J. B. Rodriguez, E. Plis, G. Bishop, Y. D. Sharma, H. Kim, L. R. Dawson, and S. Krishna, Appl. Phys. Lett. **91**, 043514 (2007).
[10]E. Plis, S. Annamalai, K. T. Posani, S. Krishna, R. A. Rupani, and S. Ghosh, J. Appl. Phys. **100**, 014510 (2005).
[11]A. Vogt, A. Simon, H. L. Hartnagel, J. Schikora, V. Buschmann, M. Rodewald, H. Fuess, S. Fascko, C. Koerdt, and H. Kurz, J. Appl. Phys. **83**, 7715 (1998).